2022

Measuement of Translucency, Biaxial Flexural Strength, and Radiopacity of Different Lithium Disilicate Materials

Preshtha Mangla
University of Alabama at Birmingham

MEASUREMENT OF TRANSLUCENCY, BIAXIAL FLEXURAL STRENGTH, AND RADIOPACITY OF DIFFERENT LITHIUM DISILICATE MATERIALS

by

PRESHTHA MANGLA

NATHANIEL C LAWSON, COMMITTEE CHAIR
FU, CHIN CHUAN
JAVED, AMJAD
ROBLES, AUGUSTO

A Thesis

Submitted to the graduate faculty of The University of Alabama at Birmingham,

in partial fulfillment of the requirements for the degree of

Master of Science

BIRMINGHAM, ALABAMA

2022

MEASUREMENT OF TRANSLUCENCY, BIAXIAL FLEXURAL STRENGTH AND RADIOPACITY AND OF DIFFERENT LITHIUM DISILICATE MATERIALS

PRESHTHA MANGLA

DENTISTRY

ABSTRACT

Objective: To measure translucency parameter, biaxial flexural strength, radiopacity and microstructure of various lithium disilicate materials used for dental restorations.

Materials and Methods: CAD/CAM lithium disilicate glass-ceramic blocks: IPS e.max CAD (Ivoclar Vivadent), CerecTessera (Dentsply Sirona), and Amber Mill (Hassbio America) were used (shade A2, HT, and MT). Blocks of each material were milled (PrograMill PM7, Ivoclar Vivadent) into cylinders (diameter = 14 mm) and cut using circular sectioning saw (IsoMET 1000 Precision Saw, Buehler) into disc-shaped specimens (thickness = 1.00 ± 0.05 mm) (n=5/group). They were hand polished to 1200 grit with SiC paper under water lubrication. The translucency parameter of uncrystallized (except IPS e.max CAD) and crystallized samples were tested against a white and black background (with glycerin gel) using a spectrophotometer (UltraScan VIS, HunterLab). A biaxial flexural strength test was performed following ISO 6872. Each specimen was placed centrally on three hardened steel balls (with a diameter of 3.2 mm, positioned 120° apart on a support circle with a diameter of 10 mm). The maximum load to fracture failure of each specimen was recorded using a universal testing machine (Instron, Model

#33R4204 Norwood, MA) with a crosshead speed of 1 mm/min. Same specimens were tested for radiopacity using the aluminum wedge. SEM analysis was also done.

<u>Results</u>: Data were analyzed using one-way ANOVA and post hoc Tukey's HSD statistical analysis ($p = 0.05$). Materials with significantly different values are denoted with different superscripts. Under SEM imaging, emax CAD demonstrated long spindle shape crystals. Tessera and Amber Mill contained finer platelet-shaped crystals and Tessera contained a virgilite phase.

Ceramic	**Translucency**	**Firing**	**Translucency Parameter**	**Biaxial Flexural Strength (MPa)**	**Radiopacity**
IPS emax® CAD	HT	Fired	30.771 ± 0.912^{b}	459.72 ± 52.39^{x}	
IPS emax® CAD	MT	Fired	29.366 ± 1.243^{bc}	396.59 ± 64.88^{xy}	0.210 ± 0.016
Cerec Tessera™	HT	Unfired	27.447 ± 0.820^{cd}		
Cerec Tessera™	HT	Fired	27.665 ± 1.284^{bcd}	299.01 ± 119.66^{xy}	
Cerec Tessera™	MT	Unfired	24.677 ± 0.187^{cd}		
Cerec Tessera™	MT	Fired	24.743 ± 0.585^{d}	344.87 ± 49.199^{xy}	0.422 ± 0.014
Amber® Mill		Unfired	45.621 ± 1.042^{a}		
Amber® Mill	HT	Fired	27.364 ± 2.548^{cd}	286.07 ± 75.93^{y}	
Amber® Mill	MT	Fired	27.641 ± 3.191^{bcd}	316.28 ± 110.41^{xy}	0.223 ± 0.008

Conclusion: Once crystallized, all lithium disilicate materials produced similar translucency despite the smaller crystalline microstructure seen in Tessera and Amber Mill. Despite the presence of an additional Virgilite phase in Tessera, it did not produce increased biaxial flexural strength. Cerec Tessera showed the highest radiopacity amongst all groups.

Keywords: Lithium Disilicate, Biaxial Flexural Strength, Microstructure, IPS Emax, Tessera, Ambermill.

DEDICATION

I dedicate my dissertation work to my family and friends. A special feeling of gratitude for my loving parents, Deepti and Satish Mangla, and my maasi, Shashi Bala, whose words of encouragement and push for tenacity ring in my ears.

I also dedicate this dissertation to my pillars of strength, my brothers Dr. Shashideep Singhal, Dr. Shashikant Singhal, Dr. Ram Prasad, and Shreshth Mangla, who have never left my side. To my sister-in-laws Dr. Shilpa Jain, Dr. Kirty Pathak, and Dr. Jyoti Aggarwal who have supported me throughout the process. I will always appreciate all they have done, for helping me to master the leadership dots.

I dedicate this work and give special thanks to my best friend Aditya Pampana for being there for me and being my best cheerleader.

ACKNOWLEDGEMENTS

I am thankful to all the people that have contributed to this project. I would like to acknowledge Dr. Nathaniel Lawson, for being a great mentor during my time in residency, as he is filled with knowledge and experience. Dr. Lawson helped me build the ideas within this thesis, performed the statistical analysis, and provided the necessary materials and specimens for this project. He always motivated me and eternally encouraged me during my residency. He gave me numerous opportunities to learn multiple treatment moralities by participating in multiple workshops and hands-on courses and assisting a clinical practice in the dental clinic. I am delighted to have him as my thesis mentor.

I would like to thank Dr. Shashikant Singhal and Dr. Thomas Hill for the initiation of this project and for being the brains behind the project.

I would like to thank Omar Nihlawi and Kelly for their constant assistance in the laboratory. They are incredible to work with, and their expertise with previous studies is greatly appreciated. I definitely learned a lot working with them.

I would like to thank Dr. Amjad Javed for helping me with all the specifics of the graduate program and for making sure I have all the paperwork and registrations required to finish the graduate program.

I would like to thank my co-residents Drs. Bushra Nizami, Krisha Shah, Chandani Mantri, Akram Gad, Ms. Hannah Bloom, and Mr. Tom Lawson for their support.

I would like to thank Ivoclar Vivadent, Dentsply Sirona, and Hassbio America for offering materials for the research.

TABLE OF CONTENTS

LIST OF FIGURES

LIST OF TABLES

LIST OF ABBREVIATIONS

Abbreviations	Ceramic	Translucency
EHT	IPS Emax	High
EMT	IPS Emax	Medium
THT (uTHT)	Cerec Tessera (Unfired Cerec Tessera)	High
TMT (uTMT)	Cerec Tessera (Unfired Cerec Tessera)	Medium
AMH (uAM)	AmberMill (Unfired AmberMill)	High
AMM	AmberMill	Medium

1. INTRODUCTION

Based on a Practice-based Research Network study, 21% of dentists preferred LDS (lithium disilicate) for posterior and 54% for anterior restorations [1]. These material preferences demonstrate the current transition from the traditional metal-ceramic restorations to those composed entirely of ceramic. The use of LDS for dental restorations was introduced in 1984 by Corning Inc [2,3]. The first glass-ceramic introduced for use in dentistry was IPS empress II by Ivoclar Vivadent in the 1990s. This ceramic was fabricated using the lost wax technique. The second generation for LDS was IPS e.max Press, fabricated using the heat press technique. Later in 2005, IPS e.max CAD was introduced. It is a machinable block and uses milling for fabrication. This material is used in dentistry for over 20 years. In the current times, there are multiple LDS materials introduced by many companies.

LDS glass-based ceramics consist of $Li_2Si_2O_5$ crystals and lithium orthophosphate (Li_3PO_4) crystals (in minor amounts) that are randomly oriented and uniformly dispersed in a glassy matrix [4]. The presence of P_2O_5 promotes volume nucleation of the lithium silicate phases by acting as a heterogeneous nucleating agent [4]. After nucleation, crystal growth occurs which imparts improved mechanical and physical properties by maximizing the presence of crystals and the generation of compression stress around the crystals [5].

There are two types of interfaces in glass-ceramics: the interface between crystalline phases and the interface between the crystalline phase and the glassy matrix [6]. The translucency of an LDS ceramic can be adjusted by varying the refractive index of the crystalline phase and the glassy matrix, and the light path at the interface between these two phases [8]. The crystalline phases of the ceramic can affect its strength. Crystals have discrete structural plans that cause deflection, branching, or splinting of cracks. The presence of these cleavage planes and grain boundaries prevents fracture propagation [7].

When preparing LDS ceramics for oral use, they require the additional processing steps of milling and post-mill crystallization [9,10]. Initially, there are small size crystals, which on exposure to heat enlarge in size. The enlarged crystals further form colonies that inter-tangle with each other. This gives this material a meshwork-like structure. Post-milling crystallization results in dendritic (tree-like or sheaf-like with significant branching) or Spherulitic (subparallel needlelike crystallites radiating from the center and forming spherical mass) morphology. These acicular structures help to achieve high strength and fracture toughness in glass-ceramics [7]. Ceramic machinability during milling is essential as low milling accuracy can cause errors in dental prostheses leading to crown-tooth margin discrepancies and clinical failure [11,12].

1.1 Ambermill

AmberMill (AM) is a nanocrystalline LDS ceramic dental material [13]. It allows multiple different translucencies to be achieved based on the post-milling crystallization parameters. This property allows clinicians to achieve translucency to match the clinical scenario with a smaller inventory of raw materials. Nucleation is controlled to limit the size of crystals, which helps control translucency [7].

1.2 IPS e.max CAD

IPS e.max CAD (IEC) is composed of 58-80% SiO□, 11-19% Li□O, 0-13% K□O, 0-8% ZrO□, 0-5% Al□0□ [4]. It is easier to mill this material when it is partially crystallized. It is purchased and milled in a partially crystallized, "blue state" [14]. As it crystallizes, the intermediate phase which consists of 40% platelet-shaped lithium metasilicate crystals embedded in a glassy phase changes to 70% fine-grain LDS crystals embedded in a glassy matrix post crystallization [15]. High strength and toughness values demonstrated by IEC [16,17,18] are due to the high crystal content (of more than 60 vol%) of LDS ceramic and interlocking microstructure.

1.3 Cerec Tessera

Introduced in March 2021, Cerec Tessera (CT) is a recent innovation in glass-ceramics technology. It contains both LDS and virgilite crystals. Virgilite is the only naturally occurring representative of the solid-solution series between β-quartz (Qz) and $LiAlSi_2O_6$ (Sp) with a stuffed β-quartz structure [19]. The virgilite crystals usually occur in parallel bands resembling flow structures [19]. Virgilite crystals are activated through the matrix firing process which adds strength and contributes to improved esthetics.

Glass-based ceramic biomaterials should be able to fulfill the functions of human teeth [20,21]. Since data regarding the translucency and biaxial flexural strength of IEC, CT, and AM are limited, this in vitro study aims to assess and compare the translucency, and biaxial flexural strength (BFS) and microstructure of recently introduced LDS materials.

2. OBJECTIVES

2.1 To Evaluate the translucency parameter of glass-ceramic materials.

The objective is to measure and compare the translucency before and after crystallization of IPS emax, Cerec Tessera, and Amber Mill.

2.2 To Evaluate the Biaxial flexural strength of glass-ceramic materials.

The objective is to measure and compare the biaxial flexural strength of Cerec Tessera and Amber Mill to IPS emax.

2.3 To Evaluate the Radiopacity of glass-ceramic materials

The objective is to measure and compare the radiopacity of Cerec Tessera and Amber Mill to IPS emax.

2.4 To analyze and evaluate the microstructure of glass-ceramic materials.

The objective is to measure and compare the microstructure of Cerec Tessera and Amber Mill to IPS emax.

3. NULL HYPOTHESES

1. There will be no difference in the **translucency of the three materials**

2. There will be no difference between the **flexural strength of the three materials**.

3. There will be no significant difference between the **radiopacity of the three materials**.

4. MATERIALS AND METHODS

4.1 Materials Used

4.1.1 Translucency Parameter: Three contemporary glass-ceramic materials with medium and high translucency

1. IPS emax - Ivoclar Vivadent
2. Cerec Terrasa – Dentsply Sirona
3. Amber Mill – Hassbio America

Table 1: Trade names and pictorial representation of lithium disilicate materials used in the study for measuring translucency.

Groups	**Classification**	**Brand**	**Translucencyand Shade**	**n**	**Manufacturer**	Pictorial Representation
Group 1	Lithium disilicate ceramic	IPS e.max® CAD	HT A2/C14	10	Ivoclar Vivadent	
Group 2	Lithium disilicate ceramic	IPS e.max® CAD	MT A2/C14	10	Ivoclar Vivadent	
Group 3 (Group 3a)	Advanced Lithium disilicate ceramic	Cerec Tessera™ (Unfired)	HT A2/C14	10	Dentsply Sirona	

						
Group 4 (Group 4a)	Advanced Lithium disilicate ceramic	Cerec Tessera™ (Unfired)	MT A2/C14	10	Dentsply Sirona	
Group 5 (Group 5a)	Nanocrystalline Lithium disilicate ceramic	Amber® Mill (Unfired)	HT A2/C14	10	Hassbio America	
Group 6	Nanocrystalline Lithium disilicate ceramic	Amber® Mill	HT A2/C14	10	Hassbio America	

4.1.2 Biaxial Flexural Strength : Three contemporary glass-ceramic materials with medium and high translucency

1. IPS emax - Ivoclar Vivadent
2. Cerec Terrasa – Dentsply Sirona
3. Amber Mill – Hassbio America

Table 2: Trade names and pictorial representation of lithium disilicate materials used in the study for measuring Biaxial flexural strength.

Groups	**Classification**	**Brand**	**Translucencyand Shade**	**n**	**Manufacturer**	Pictorial Representation
Group 1	Lithium disilicate ceramic	IPS e.max® CAD	HT A2/C14	10	Ivoclar Vivadent	
Group 2	Lithium disilicate ceramic	IPS e.max® CAD	MT A2/C14	10	Ivoclar Vivadent	
Group 3 (Group 3a)	Advanced Lithium disilicate ceramic	Cerec Tessera™ (Unfired)	HT A2/C14	10	Dentsply Sirona	

Group 4 (Group 4a)	Advanced Lithium disilicate ceramic	Cerec Tessera™ (Unfired)	MT A2/C14	10	Dentsply Sirona	
Group 5 (Group 5a)	Nanocrystalline Lithium disilicate ceramic	Amber® Mill (Unfired)	HT A2/C14	10	Hassbio America	
Group 6	Nanocrystalline Lithium disilicate ceramic	Amber® Mill	HT A2/C14	10	Hassbio America	

4.1.3 Radiopacity : Three contemporary glass-ceramic materials with medium and high translucency

1. IPS emax - Ivoclar Vivadent
2. Cerec Terrasa – Dentsply Sirona
3. Amber Mill – Hassbio America

Table 3: Trade names and pictorial representation of lithium disilicate materials used in the study for measuring radiopacity.

Material Name	**Material Type**	**Manufacturer**	n	Pictorial representation
IPS Emax CAD	Glass Ceramic	Ivoclar Vivadent	9	
Cerec Tessera	Glass Ceramic	Densply Sirona	9	
AmberMill	Glass Ceramic	Hassbio America	9	

4.2 Method

4.2.1 Specimen preparation

The experimental groups included LDS glass-ceramics: IPS e.max CAD (Ivoclar Vivadent), Cerec Tessera (Dentsply Sirona), and AmberMill (Hassbio America) in this study (Table.1). Translucencies compared were High Translucency (HT) and Medium Translucency (MT). A2 shade was used for all the ceramics. Blocks of size C14 were milled into cylinders of a diameter of 14 mm using PrograMill PM7 (Ivoclar Vivadent). Disc-shaped test specimens with a diameter of 14 mm and a thickness of 1 ± 0.05 mm were fabricated from 14×12×18 mm cylinders using the sectioning saw from IsoMET 1000 Precision Saw, Buehler.

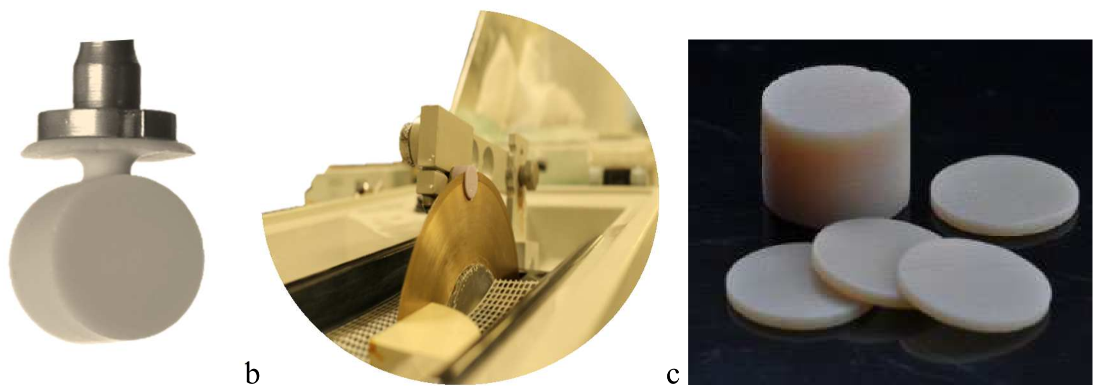

a b c

Figure 1: Specimen Preparation a) Milled Block b) Specimen placed in saw c) Disc Shaped specimen

4.2.2 Surface treatment

All samples were hand polished using silicon carbide sandpaper on a polishing wheel, up to 1200 grit on one side and 320 grit on the other side for translucency parameter analysis. For BFS, samples were polished up to 600 grits on one side and 320 grits on the other. They were polished under water lubrication.

Figure 2: Polishing under water lubrication

4.2.3 Translucency measurement

Color measurements were taken using a spectrophotometer (UltraScan PRO Spectrophotometer HunterLab) before and after crystallization (except). Crystallization was done as per the manufacturer's recommendation using a Programmat furnace (Ivoclar Vivadent). L*a*b* color parameters were recorded in the spectrophotometer against black and white tiles. A thin layer of glycerine was placed between the specimens and the tiles. The difference in color recorded against the black and white backgrounds was used to calculate the translucency parameter (TP), and the contrast ratio (CR) using the formula:

$$TP = [(L_b - L_w)^2 + (a_b - a_w)^2 + (b_b - b_w)^2]^{½}$$

$$CR = L_B / L_W$$

a

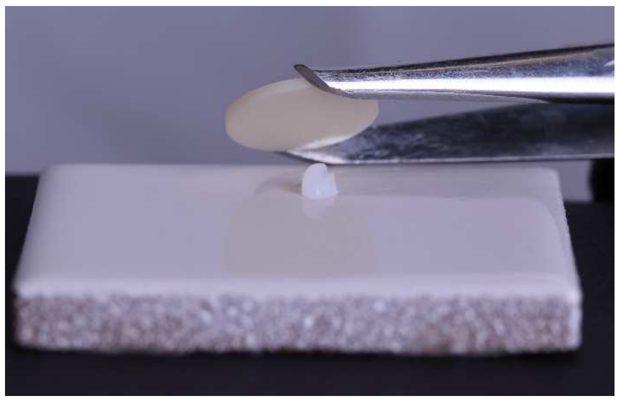
b


c

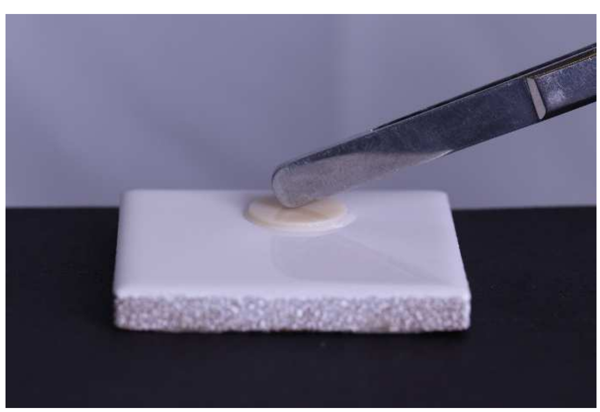
d

Figure 3: Translucency measurement a) glycerine gel b) specimens placed against white tile c) specimens placed against black tile d) final position of specimen on tile

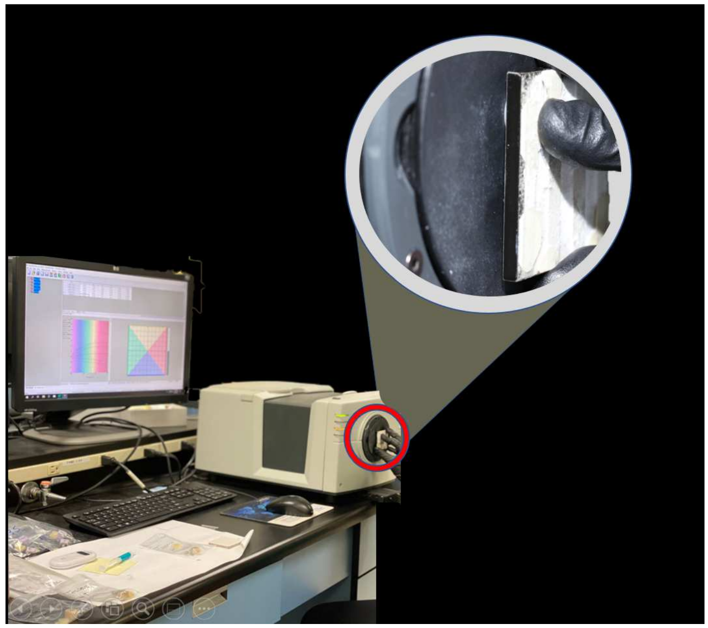

Figure 4: Spectrophotometer used.

4.2.4 Biaxial Flexural strength

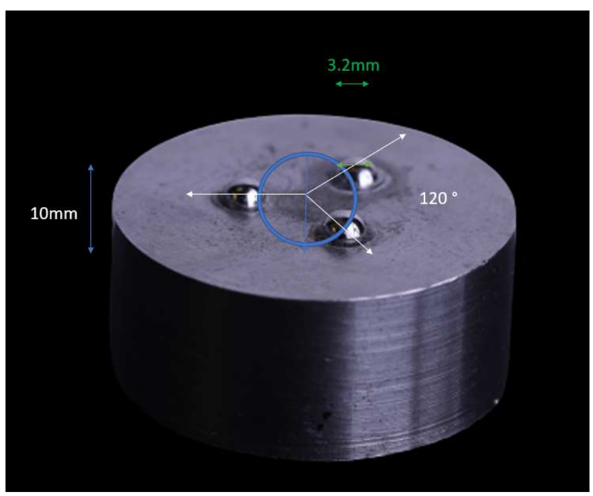

Figure 5: Metal block used for placing disc specimen.

The BFS was performed according to DIN EN ISO 6872:2019[11]. Each specimen was placed centrally on three hardened steel balls [with a diameter of 3.2 mm (figure 2), positioned 120° apart on a support circle with a diameter of 10 mm. A 1.8 mm tip steel indenter applied force to the center of the disc at a rate of 1 mm/min. The maximum load to fracture failure of each specimen was recorded using a universal testing machine (Instron, Model #33R4204, Noorwood, MA).

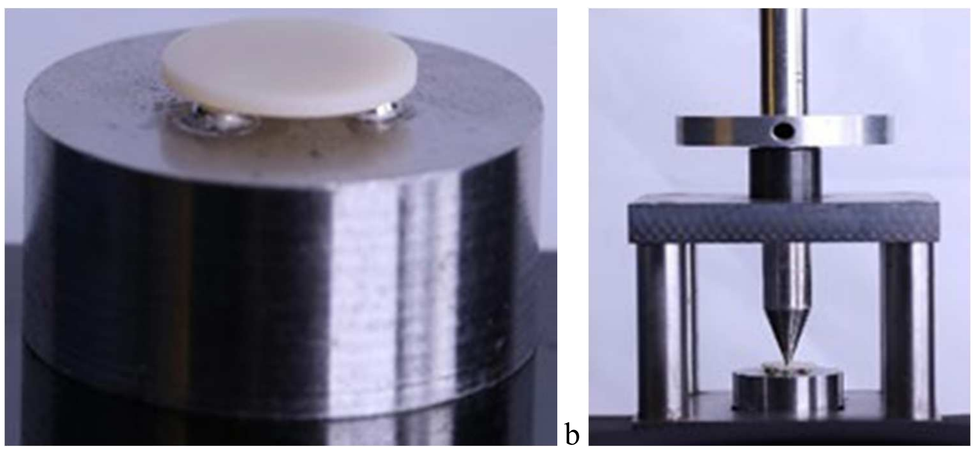

a b

Figure 6: Measurement of biaxial flexural strength a) specimen on supports b) indentor placed on top of specimen

4.2.5 Radiopacity

The radiopacity of the specimens was compared by measuring the radiodensity of the materials on digital radiographs. The specimens were radiographed with a digital x-ray device (Planmeca; Prostyle Intra) set at 70 kVp for 0.32 seconds along with an aluminum step wedge. A standardized radiograph of the specimens will be made using an occlusal film 41.15×30.99 mm and the processed film will then be scanned with a digital imaging system (Scan-X 1/0; Air Techniques Inc). Each step of the aluminum wedge represents an equivalent 1-mm thickness of pure aluminum that will be converted into values of radiopacity. Image analysis software (Photoshop; Adobe Systems Inc) will be used to measure the gray scale levels of the ceramics using the Histogram function and to compare intensity values to the step wedge. The material should have an equivalent radiopacity to 2mm of aluminum in order to be considered radiopaque.

a

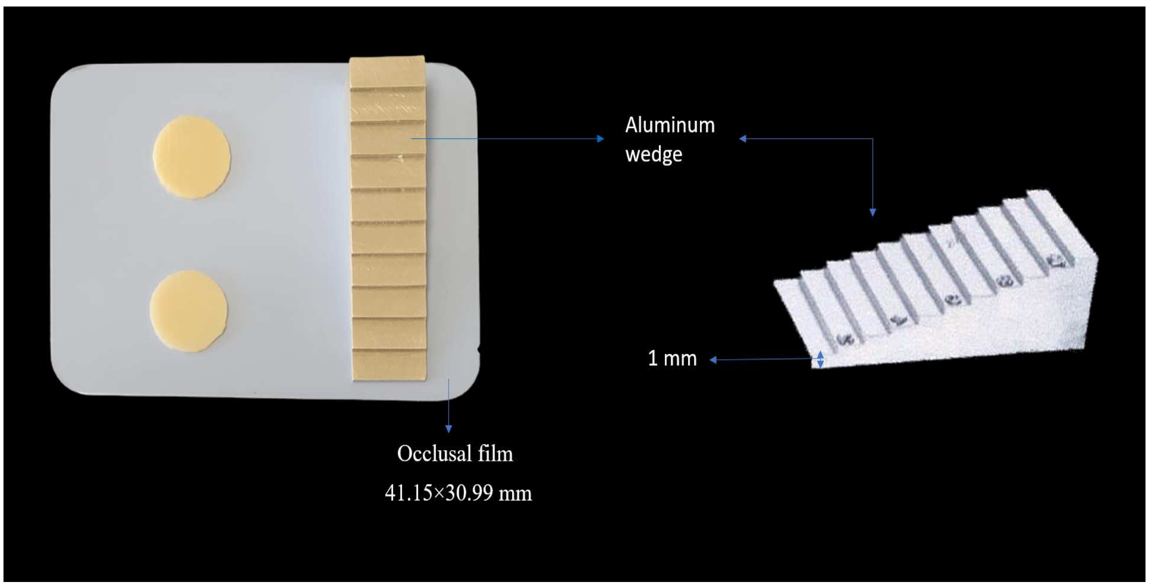

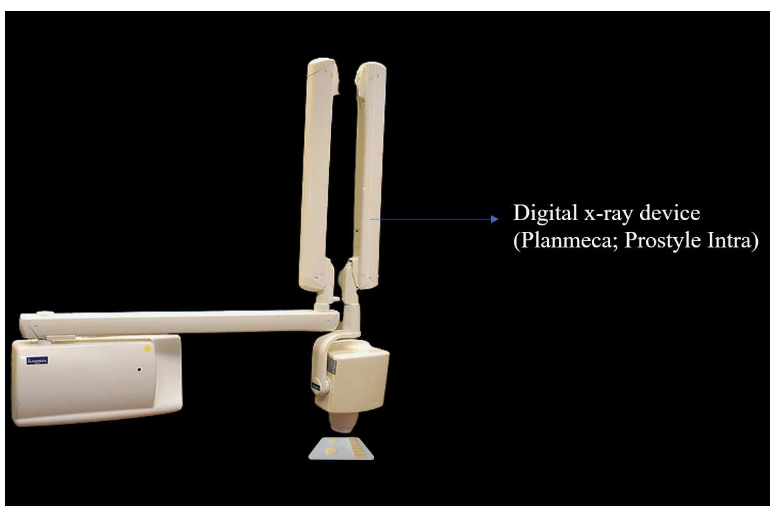

b

c 

Figure 7: Measurement of Radiopacity using Aluminium Wedge a) specimen placed on digital film with aluminum step wedge, b) x-ray positioned above specimen, c)processor

4.2.6 Microstructure analysis

The specimens were cleaned in ethanol, secured to tabs with gold conducting tape, and gold-coated in a vacuum sputter coater. The specimens were examined in a scanning electron microscope (SEM) (Quanta FEG 650, FEI) using the secondary electron imaging mode.


Cleaned in ethanol

a

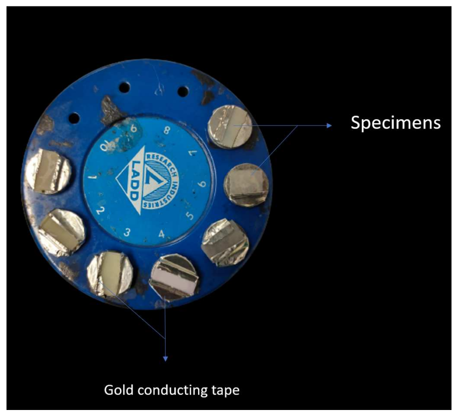
Specimens
Gold conducting tape

b

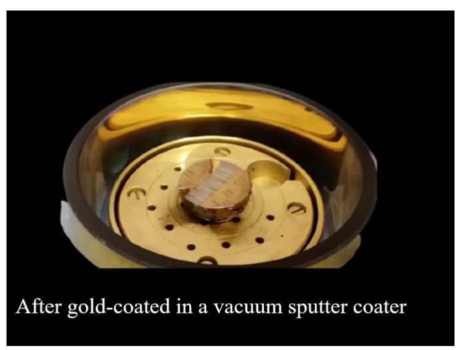
After gold-coated in a vacuum sputter coater

c

d 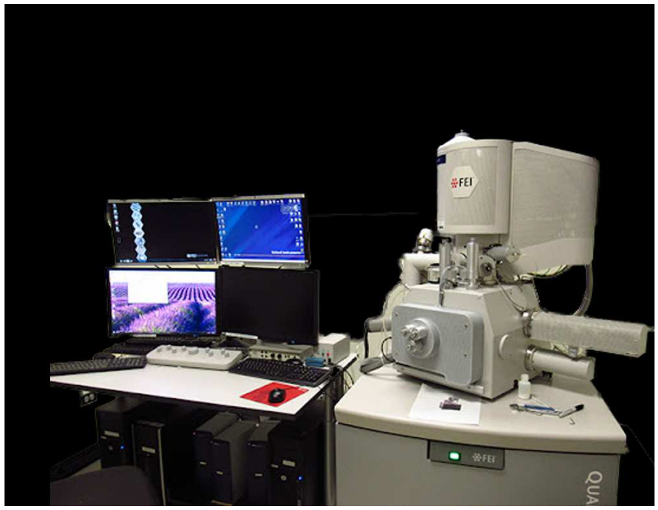

Scanning electron microscope (SEM) (Quanta FEG 650, FEI)

Figure 8: Microstructure analysis a) specimen cleaning b) placement on tray, c) gold coating specimens, d) specimens examined in SEM

5. STATISTICAL ANALYSIS

Differences between groups were analyzed by one-way analysis of variance (ANOVA), and Tukey's test was used for multiple comparisons in the case of a difference among groups. For all tests, the level of significance was set at $p < 0.05$, and SPSS Statistic 27.0.1 software (IBM Inc., Armonk, NY, USA) was used.

6. RESULTS

There were significant differences in the TP and BFS of experimental samples ($p<0.05$). Tukey's analysis showed that some study groups were statistically significant from others. Detailed results are shown in Table 2. Materials with significantly different values are denoted with different superscripts. Under SEM imaging, IEC demonstrated long spindle shape crystals. CT and AM contained finer platelet shaped crystals and CT contained a virgilite phase.

6.1.1 Values

Table 4: Results

Ceramic	Contrast Ratio	Translucency Parameter	Biaxial Flexural Strength (MPa)	Radiopacity
EHT	0.354 ± 0.014^{q}	30.771 ± 0.912^{b}	459.72 ± 52.39^{x}	
EMT	0.394 ± 0.022^{q}	29.366 ± 1.243^{bc}	396.59 ± 64.88^{xy}	0.210±0.016
THT (uTHT)	0.530 ± 0.023r (0.535 ±	27.665 ± 1.284^{bcd} (27.447 ± 0.820^{cd})	299.01 ± 119.66^{xy}	

	0.017) r			
TMT (uTMT)	0.597 ± 0.012^{s} (0.602 ± 0.004) ^{q}	24.743 ± 0.585^{d} (24.677 ± 0.187c^{d})	344.87 ± 49.199^{xy}	0.422±0.014
AMH (uAMH)	0.534 ± 0.043^{r} (0.179 ± 0.005) ^{p}	27.364 ± 2.548^{cd} (45.621 ± 1.042^{a})	286.07 ± 75.93^{y}	
AMM	0.524 ± 0.049 ^{r}	27.641 ± 3.191^{bcd}	316.28 ± 110.41^{xy}	0.223±0.008

*values with different superscripts in each column are statistically different

6.1 Results for Translucency

Table 5: Results for translucency parameter.

									Translucency Parameter		
	ID	L*	a*	b*	Y	x	y		TP	Average	SD
Amber Mill - unfired	1b	34.91	-0.77	-8.64	8.45	0.2792	0.2976				
	1w	75.02	0.35	14.76	48.3	0.3459	0.3638		46.450		
	2b	35.54	-0.93	-8.78	8.77	0.2786	0.2976				
	2w	75.13	0.04	14.28	48.48	0.3443	0.363		45.827		
	3b	36.36	-1.11	-8.69	9.2	0.279	0.2987				
	3w	77.01	-0.04	7.8	51.56	0.33	0.3482		43.880		
	4b	35.82	-0.88	-8.58	8.91	0.2797	0.2985				
	4w	74.71	0.48	15.12	47.82	0.347	0.3646		45.563		
	5b	35.46	-0.83	-8.46	8.73	0.28	0.2987				
	5w	75.95	0.34	14.14	49.8	0.3442	0.3622		46.385	**45.621**	1.042
Amber Mill - MT	1b	61.08	-5.06	-3.79	29.34	0.2947	0.3254				
	1w	78.63	0.8	15.6	54.3	0.3471	0.364		26.801		
	2b	57.24	-4.79	-6.08	25.17	0.2883	0.3183				
	2w	79.23	0.51	16.11	55.32	0.3475	0.3651		31.687		
	3b	58.99	-5.24	-4.87	27.02	0.2911	0.3224				
	3w	77.76	0.65	16	52.81	0.348	0.3653		28.680		
	4b	59.98	-5.08	-4.85	28.1	0.2917	0.3224				
	4w	78.42	0.71	15.58	53.93	0.347	0.3641		28.124		
	5b	63.0	-	-	31.6	0.303	0.333				

		9	4.65	0.81	9	1	1				
	5w	78.21	0.59	15.59	53.57	0.3469	0.3643		22.914	**27.641**	3.191
Amber Mill - HT	1b	61.92	-5.31	-3.98	30.31	0.2939	0.3252				
	1w	78.56	0.56	14.81	54.16	0.3451	0.3625		25.776		
	2b	61.85	-5.12	-2.88	30.22	0.2969	0.328				
	2w	76.97	0.66	14.99	51.49	0.3462	0.3634		24.111		
	3b	60.04	-5.36	-5.41	28.16	0.2898	0.3211				
	3w	77.48	0.47	14.73	52.33	0.3452	0.3628		27.272		
	4b	58.85	-5.06	-5.89	26.87	0.2888	0.3194				
	4w	78.07	0.62	15.39	53.33	0.3466	0.3639		29.232		
	5b	57.87	-5.04	-7.08	25.83	0.2855	0.3159				
	5w	78.32	0.41	14.78	53.76	0.3449	0.3627		30.426	**27.364**	2.548
Tessera HT unfired	1b	59.39	-3.9	-3.8	27.45	0.2965	0.3242				
	1w	77.16	2.45	16.72	51.81	0.3528	0.3653		27.878		
	2b	58.68	-3.72	-3.32	26.68	0.2979	0.3253				
	2w	77.6	2.42	17.32	52.53	0.3538	0.3665		28.665		
	3b	59.76	-4	-3.07	27.86	0.2982	0.3263				
	3w	76.45	2.66	16.66	50.62	0.3533	0.3653		26.687		
	4b	59.74	-3.84	-3.13	27.83	0.2983	0.326				
	4w	76.81	2.58	16.58	51.21	0.3528	0.365		26.853		
	5b	59.57	-3.98	-3.37	27.65	0.2974	0.3255				
	5w	76.56	2.6	16.76	50.81	0.3534	0.3655		27.151	**27.447**	0.820
Tessera MT unfired	1b	62.3	-4.15	-0.42	30.75	0.3049	0.3337				
	1	76.9	3.1	18.2	51.4	0.357	0.368		24.82		

	w	5		7	4	2	1		9		
	2b	62.12	-4.2	-0.59	30.54	0.3043	0.3333				
	2w	76.37	3	18.24	50.49	0.3572	0.3684		24.687		
	3b	62.35	-4.31	-0.2	30.82	0.3051	0.3344				
	3w	76.61	3.02	18.17	50.88	0.357	0.3681		24.383		
	4b	62.22	-4.18	-0.42	30.66	0.3048	0.3337				
	4w	76.9	2.92	18.05	51.36	0.3564	0.3678		24.638		
	5b	62.69	-4.33	-0.32	31.22	0.3048	0.3341				
	5w	77.15	2.97	18.52	51.79	0.3574	0.3687		24.846	**24.677**	0.187
Tessera HT fired	1b	59.75	-3.92	-3.4	27.85	0.2975	0.3254				
	1w	76.94	2.32	16.68	51.43	0.3526	0.3655		27.160		
	2b	60	-3.94	-2.79	28.12	0.299	0.3271				
	2w	77.22	2.39	16.88	51.9	0.3529	0.3657		26.898		
	3b	58.33	-3.94	-4.32	26.31	0.2948	0.3227				
	3w	77.99	2.2	17.12	53.2	0.3528	0.3661		29.730		
	4b	60.26	-4.01	-2.72	28.41	0.2992	0.3274				
	4w	76.88	2.48	16.88	51.33	0.3533	0.3657		26.505		
	5b	59.17	-3.9	-3.86	27.21	0.2963	0.324				
	5w	77.42	2.18	16.53	52.23	0.3518	0.3651		28.032	**27.665**	1.284
Tessera MT fired	1b	62.2	-4.15	-0.37	30.64	0.305	0.3338				
	1w	76.6	2.54	18.31	50.88	0.3564	0.3689		24.516		
	2b	62.79	-4.24	0.08	31.34	0.306	0.3351				
	2w	76.83	2.62	18.28	51.25	0.3564	0.3686		23.988		
	3b	61.7	-	-	30.1	0.303	0.332				

		5	4.15	0.84	1	8	6				
	3w	77.18	2.66	18.34	51.83	0.3565	0.3686		25.541		
	4b	62.34	-4.27	-0.38	30.8	0.3047	0.3339				
	4w	77.39	2.65	18.41	52.19	0.3565	0.3687		25.049		
	5b	62.51	-4.21	-0.23	31	0.3052	0.3343				
	5w	77.06	2.88	18.32	51.63	0.3568	0.3684		24.619	**24.743**	0.585
emax HT	1b	50.53	-1.64	-0.61	18.86	0.3084	0.3309				
	1w	77.8	0.51	13.29	52.87	0.3422	0.3595		30.684		
	2b	50.26	-1.65	-0.6	18.64	0.3084	0.3309				
	2w	77.11	0.45	13.3	51.72	0.3423	0.3598		30.307		
	3b	50.91	-1.72	-0.59	19.19	0.3083	0.331				
	3w	77.05	0.43	13.26	51.62	0.3422	0.3598		29.660		
	4b	49.69	-1.58	-0.59	18.16	0.3085	0.3309				
	4w	77.47	0.47	13.25	52.32	0.3421	0.3596		31.104		
	5b	49.37	-1.59	-0.88	17.9	0.3076	0.33				
	5w	78.2	0.46	13.08	53.55	0.3415	0.359		32.098	**30.771**	0.912
emax MT	1b	51.22	-1.81	-0.24	19.46	0.3091	0.3322				
	1w	78.4	0.71	15.06	53.89	0.3459	0.363		31.292		
	2b	53.64	-1.93	0.55	21.64	0.3112	0.3346				
	2w	77.75	0.74	15.5	52.78	0.3471	0.3641		28.494		
	3b	52.57	-1.94	0.27	20.65	0.3103	0.3338				
	3w	78.39	0.66	15.22	53.88	0.3462	0.3634		29.949		
	4b	53.66	-1.99	0.35	21.65	0.3105	0.3341				
	4	78.0	0.7	15.2	53.2	0.346	0.363		28.66		

	w	1		4	3	4	5		8		
	5b	53.78	-1.91	0.71	21.77	0.3117	0.3351				
	5w	77.9	0.77	15.51	53.05	0.3471	0.3641		28.425	**29.366**	1.243

6.1.2 Graphical representation of data:

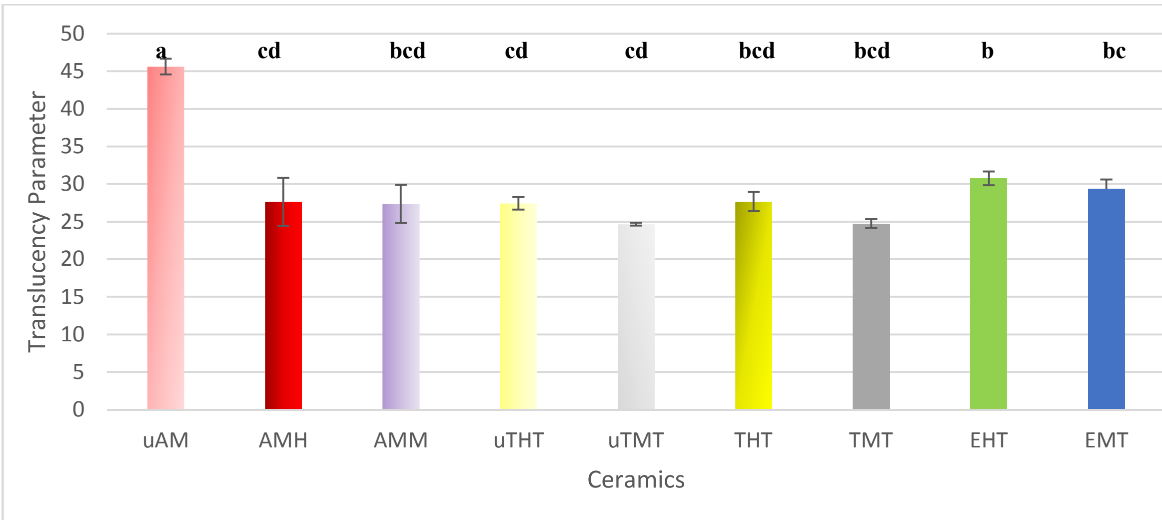

Graph 1: Translucency parameters of ceramic.

6.1.3 Statistical analysis

ANOVA

TP

	Sum of Squares	df	Mean Square	F	Sig.
Between Groups	1615.077	8	201.885	79.559	<.001
Within Groups	91.352	36	2.538		
Total	1706.429	44			

Figure 9: Anova output for translucency parameter of ceramics.

TP

Tukey HSD[a]

Ceramic	N	Subset for alpha = 0.05			
		1	2	3	4
Cerec HT unfired	5	24.6766			
Cerec HT fired	5	24.7426			
Ambermill HT	5	27.3634	27.3634		
Cerec MT unfired	5	27.4468	27.4468		
Ambermill MT	5	27.6412	27.6412	27.6412	
Cerec MT fired	5	27.6650	27.6650	27.6650	
Emax HT	5		29.3656	29.3656	
Emax MT	5			30.7706	
Ambermill unfired	5				45.6210
Sig.		.106	.561	.078	1.000

Means for groups in homogeneous subsets are displayed.

a. Uses Harmonic Mean Sample Size = 5.000.

Figure 10: Tukey output for translucency parameter of ceramics.

6.2 Results for Biaxial Flexural Strength

6.2.1 Values

Table 6a: Biaxial flexural strength for IPS emaax

Specimen	thickness (b)	r1	r2	r3	v - Poison's Ratio	X	Y	P - failure load (N)	of - Fracture strength (MPa)
1	0.95	11	1.4	14	0.25	-5.75271	1.110105	229.31	416.2274
2	1.01	11	1.4	14	0.25	-5.75271	1.110105	242.91	390.0835
3	0.99	11	1.4	14	0.25	-5.75271	1.110105	199.2	332.946
4	1.04	11	1.4	14	0.25	-5.75271	1.110105	253.9	384.5483
5	0.96	11	1.4	14	0.25	-5.75271	1.110105	200.6	356.5688

6	1.04	11	1.4	14	0.25	-5.75271	1.110105	267.3	404.8435
7	1.05	11	1.4	14	0.25	-5.75271	1.110105	419.67	623.5686
8	1.05	11	1.4	14	0.25	-5.75271	1.110105	327.73	486.9591
9	1.01	11	1.4	14	0.25	-5.75271	1.110105	219.69	352.795
10	0.98	11	1.4	14	0.25	-5.75271	1.110105	185.69	316.7315
Average									406.5272
Standard Deviation									90.23863

Table 6b: Biaxial flexural strength for AmberMill

Specimen	thickness (b)	r1	r2	r3	v - Poison's Ratio	X	Y	P - failure load (N)	σf - Fracture strength (MPa)
1	0.97	11	1.4	14	0.25	-5.75271	1.110105	188.24	327.7354
2	1.07	11	1.4	14	0.25	-5.75271	1.110105	299.75	428.8906
3	1	11	1.4	14	0.25	-5.75271	1.110105	185.87	304.4838
4	1.06	11	1.4	14	0.25	-5.75271	1.110105	291.55	425.0658
5	0.95	11	1.4	14	0.25	-5.75271	1.110105	227.97	413.7951
6	1.04	11	1.4	14	0.25	-5.75271	1.110105	279.18	422.8365
7	1	11	1.4	14	0.25	-5.75271	1.110105	254.45	416.8284
8	0.97	1	1.	1	0.25	-	1.110	226.03	393.5297

		1	4	4		5.75271	105		
9	1.04	11	1.4	14	0.25	-5.75271	1.110105	315.48	477.8153
10	1.05	11	1.4	14	0.25	-5.75271	1.110105	260.43	386.9611
Average									399.7942
Standard deviation									50.62955

Table 6c: Biaxial flexural strength for Cerec Tessera

Specimen	thickness (b)	r1	r2	r3	ν - Poison's Ratio	X	Y	P - failure load (N)	σf - Fracture strength (MPa)
1	1	11	1.4	14	0.25	-5.75271	1.110105	184.35	301.9938
2	1.04	11	1.4	14	0.25	-5.75271	1.110105	270.08	409.054
3	1.01	11	1.4	14	0.25	-5.75271	1.110105	189.46	304.2494
4	1.03	11	1.4	14	0.25	-5.75271	1.110105	204.25	315.3861
5	1.05	11	1.4	14	0.25	-5.75271	1.110105	242.23	359.9185
6	1.01	11	1.4	14	0.25	-5.75271	1.110105	218.43	350.7716
7	1.01	11	1.4	14	0.25	-5.75271	1.110105	158.08	253.857
8	1.05	11	1.4	14	0.25	-5.75271	1.110105	186.78	277.5279
9	0.96	11	1.4	14	0.25	-5.75271	1.110105	197.75	351.5029
10	0.97	11	1.4	14	0.25	-5.75271	1.110105	137.87	240.0387

Average									316.43
Std Dev.									52.17723

6.2.2 Graph

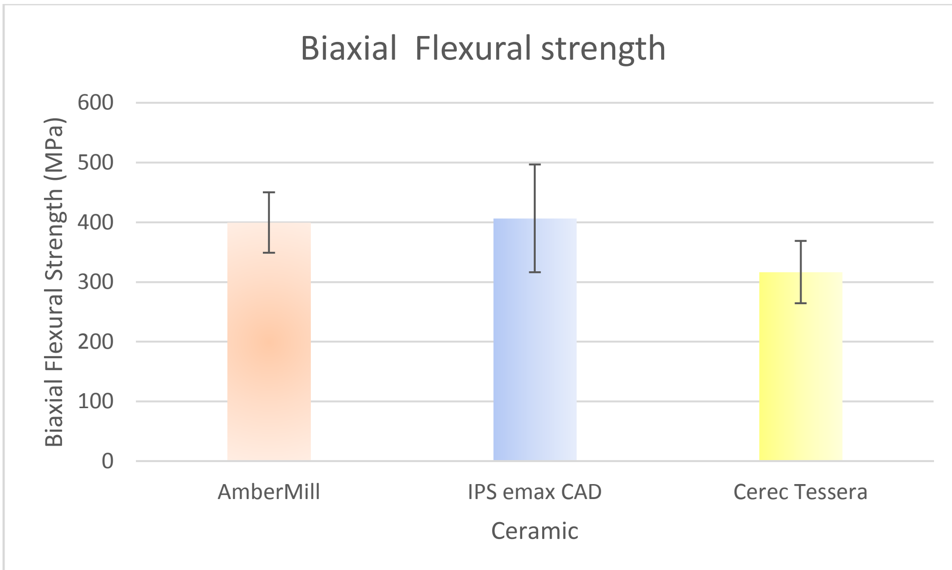

Graph 2: Biaxial Flexural strength of ceramics

6.2.3 Statistical analysis

ANOVA

Biaxialflexuralstrength

	Sum of Squares	df	Mean Square	F	Sig.
Between Groups	50374.739	2	25187.369	5.627	.009
Within Groups	120859.420	27	4476.275		
Total	171234.159	29			

Figure 11: Anova Output for biaxial flexural strength of ceramics.

Biaxialflexuralstrength

Tukey HSD[a]

Ceramic	N	Subset for alpha = 0.05

		1	2
Cerec tessera	10	316.4300	
AmberMill	10		399.7942
IPS emax	10		406.5272
Sig.		1.000	.972

Means for groups in homogeneous subsets are displayed.

a. Uses Harmonic Mean Sample Size = 10.000.

Figure: 12: Tukey test output for biaxial flexural strength of ceramics.

6.3 Results for Radiopacity

6.3.1 Values

Table 7a: Radiopacity results for AmberMill

S.No	Radiopacity
1	0.226
2	0.235
3	0.223
4	0.236
5	0.224
6	0.229
7	0.214
8	0.21
9	0.218
Avg	0.223889
std.	0.008852

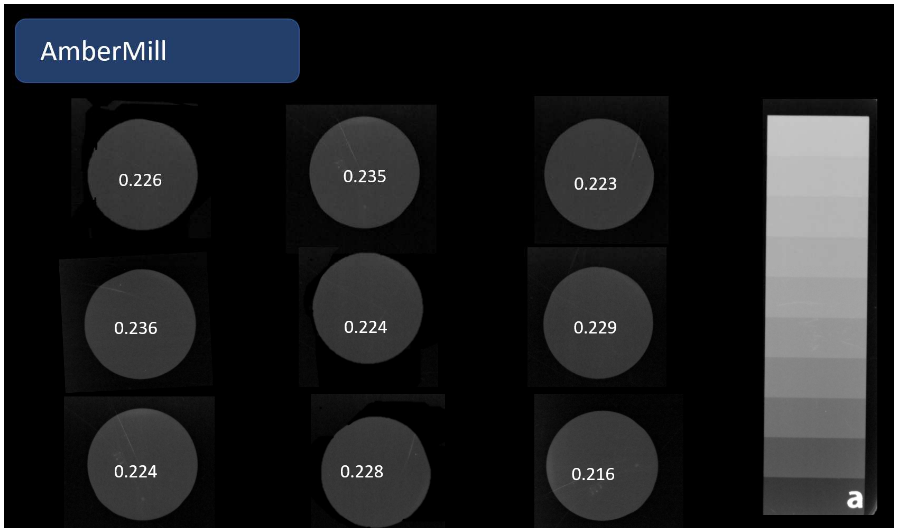

Figure 13a Ceramic specimens (AmberMill) with aluminium wedge for comparing radiopacity.

Table 7b: Radiopacity results for IPS e.max CAD

S.No	Radiopacity
1	0.209
2	0.197
3	0.232
4	0.233
5	0.232
6	0.24
7	0.212
8	0.194
9	0.219
Avg.	0.218667
Std.	0.016703

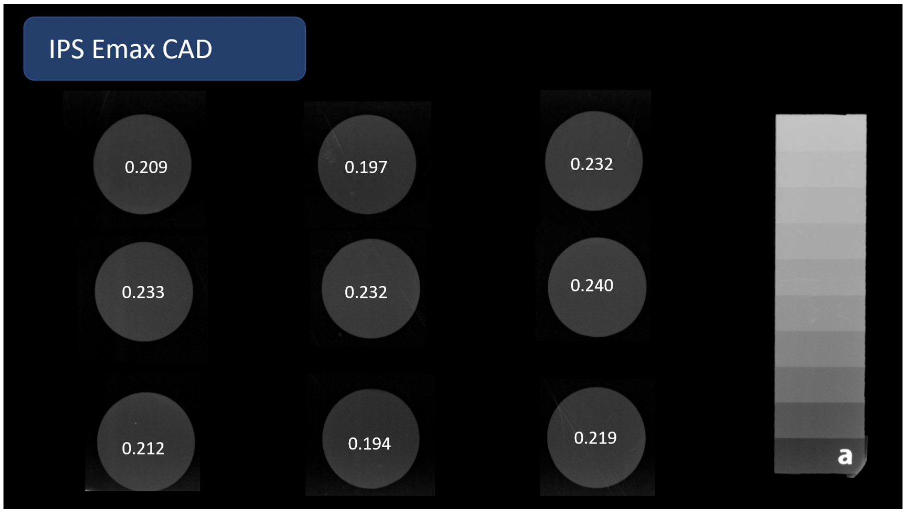

Figure 13b Ceramic specimens (IPS e.max CAD) with aluminium wedge for comparing radiopacity.

Table 7c: Radiopacity results for Cerec Tessrea

S.No	Radiopacity
1	0.408
2	0.414
3	0.4
4	0.423
5	0.421
6	0.432
7	0.422
8	0.45
9	0.432
Avg	0.422444
std.	6980.014

Figure 13c Ceramic specimens (Cerec Tessera) with aluminium wedge for comparing radiopacity.

6.3.2 Graph

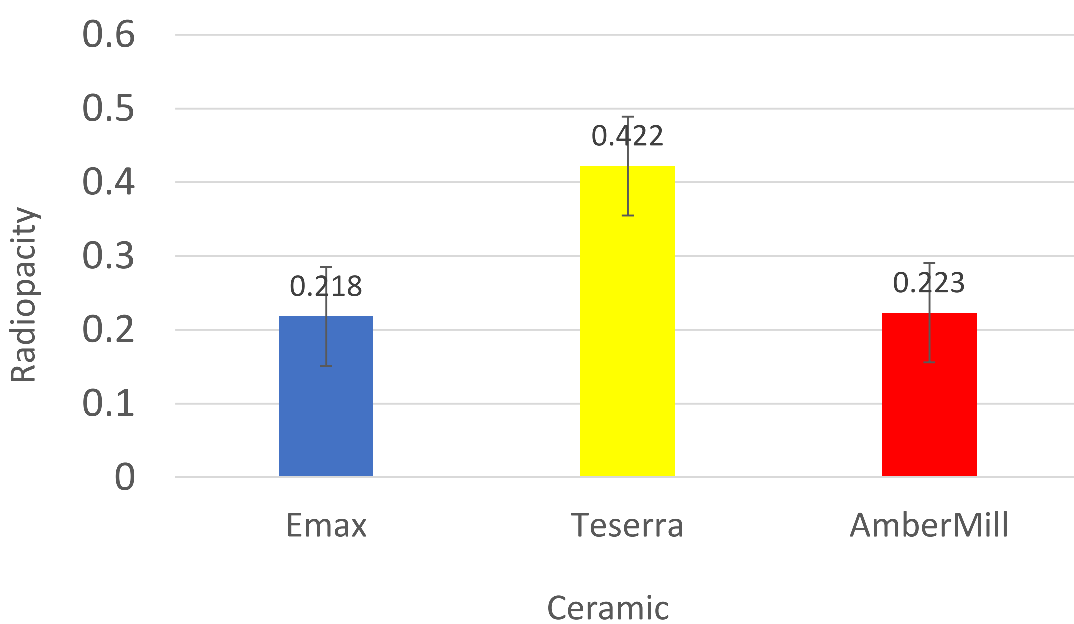

Graph 3 : Radiopacity of ceramics

6.3.3 Statistical Analysis

ANOVA

Radiopacity

	Sum of Squares	df	Mean Square	F	Sig.
Between Groups	.243	2	.121	635.513	<.001
Within Groups	.005	24	.000		
Total	.248	26			

Figure 14: One-way ANOVA output for radiopacity of ceramics.

Radiopacity

Tukey HSD[a]

		Subset for alpha = 0.05	
Ceramic	N	1	2
IPS e.max	9	.2187	
AmberMill	9	.2239	
Cerec Tessera	9		.4224
Sig.		.706	1.000

Means for groups in homogeneous subsets are displayed.

a. Uses Harmonic Mean Sample Size = 9.000.

Figure 15 : Tukey test output for radiopacity of ceramics.

7. NULL HYPOTHESES REJECTION

There were statistically significant difference between the translucency, biaxial flexural strength, and radiopacity of the three ceramic materials. Thus the null hypothesis is rejected.

8. DISCUSSION

The development of lithium disilicate, zirconia, and alumina-reinforced ceramics has allowed the substitution of metallic infrastructures in diverse clinical situations, due to their high flexural and compressive strength [22]. The present study was undertaken to compare various commercially available contemporary glass ceramics for their translucency and flexural strength. High and medium translucencies for the A2 shade of IEC, CT, and AM were compared. The result of this study leads to the rejection of the null hypothesis.

Calculation of the translucency parameter is one of the most common approaches to evaluating light interactions in a dental restorative material [23]. Heffernan et al [24,25,26] showed that different crystalline compositions result in a range of translucencies of ceramics at clinically relevant thicknesses. Our study confirms these results as ceramics with different microstructures showed variation in the translucencies. In AM, crystals are nano size and small crystal size gives high translucency. Limiting the grain size increases the density of the crystals and decreases the grain boundaries to increase translucency [27]. CT contains virgilite crystals which has been proposed to improve its translucency. But based on the current study, CT showed the lowest translucency amongst all groups. The high translucency of IEC is credited to a similar refractive index of the lithium disilicate crystalline phase and the glassy phase [28]. This interface is responsible for the light scattering properties of this material. Increasing the crystallinity percentage of the ceramic improves mechanical properties but compromises translucency and color of the material [14,28].

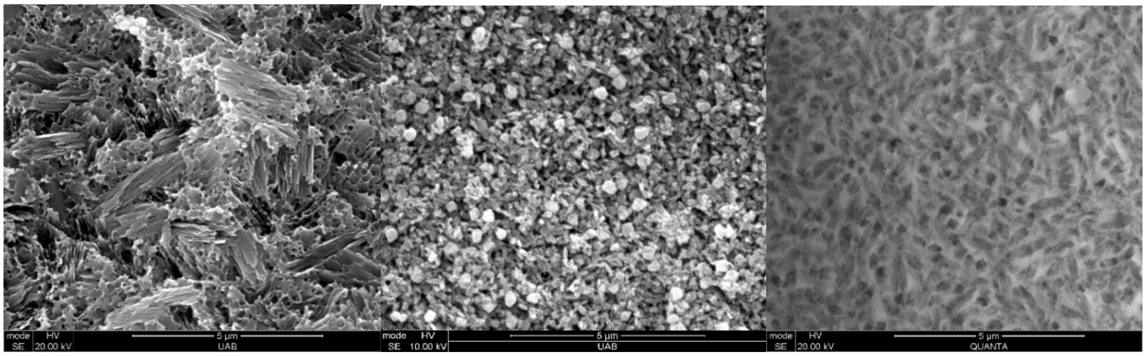

Figure 16: (left to right) IPS e.max CAD, Cerec Tessera, AmberMill

As per ISO standards 6872, uniaxial tests (three-point bending and four-point bending) and biaxial flexure (piston-on-three-ball) are accepted for measuring flexural strength. Uniaxial flexural strength tests use beam-shaped specimens which often have edge flaws [29]. These flaws act as the site for stress concentration and lead to undesirable edge failures. Therefore, the fracture is due to edge failure instead of a fracture that originates from the intrinsic flaw of the material [30,31]. Studies have shown biaxial flexural strength test is more sensitive than uniaxial flexural strength tests (ceramics [32], glass ionomer cements [33], composites [34,35]). Thus, biaxial flexural strength test was selected for this study.

Microstructure analysis of IEC gave a meshwork-like appearance. The crystals enlarge from nano-size crystals to form colonies. These colonies form layers, eventually resulting in highly intertwined colonies. This complex structure is difficult to break and is the main reason for its high flexural strength. A material with high flexural strength can chip during the milling procedure. Therefore, it is available partially crystalized for easy milling. After full crystallization, it achieves high flexural strength. CT showed lower flexural strength than mentioned by the manufacturer. It is fired at a lower temperature (760ºC) which might have hindered the crystal growth eventually affecting its flexural strength. AM has nano-sized crystals which may have allowed a crack to propagate resulting in lower flexural strength.

Various studies have analyzed the translucency and flexural strength of IEC as it is one of the oldest CAD/CAM ceramics available. Studies by Eldwakhly et al [36] and Liebermann et al [37] showed high translucency of IEC as compared to other contemporary ceramics. Apel et al. [38] and Stawarczyk et al [39] have shown flexural strength values of IEC around 430 MPa using the biaxial flexural test. These values are similar to our study. Alberto et al reported a flexural strength for IEC as 271.6 ± 64.7 MPa using a 3-point bend flexural strength testing conditions [40]. Further conclusions regarding the results achieved are hampered by the fact that detailed information on the compositions was not available for CT or AM. There is only one comparable investigation of the tested CAD/CAM ceramics (AM and CT) in the literature [37].

9. CONCLUSION

Once crystallized, all lithium disilicate materials produced similar translucency despite the smaller crystalline microstructure seen in CT and AM Despite the presence of an additional virgilite phase in CT, it did not produce increased biaxial flexural strength. The general ranking of the TP for the fired glass ceramics was

EHT > EMT > THT > AMM > AMH > TMT

BFS was

EHT > EMT > TMT > AMM > THT > AMH

Radiopacity was

TMT>AMM>EMT

10. REFERENCES

[1] Makhija SK, Lawson NC, Gilbert GH, Litaker MS, McClelland JA, Louis DR, Gordan VV, Pihlstrom DJ, Meyerowitz C, Mungia R, McCracken MS; National Dental PBRN Collaborative Group. Dentist material selection for single-unit crowns: Findings from the National Dental Practice-Based Research Network. J Dent. 2016 Dec;55:40-47.

[2] El-Meliegy E., van Noort R. Glasses and Glass Ceramics for Medical Applications. Springer; New York, NY, USA: 2012. Machinable mica dental glass-ceramics; pp. 1–244.

[3] Ritzberger C., Apel E., Höland W., Peschke A., Rheinberger V.M. Properties and clinical application of three types of dental glass-ceramics and ceramics for CAD-CAM technologies. Materials. 2010;3:3700–3713.

[4] Manjeet S. Dahiya, Vijay K. Tomer, S. Duhan, Bioactive glass/glass ceramics for dental applications, Editor(s): Abdullah M. Asiri, Inamuddin, Ali Mohammad, In Woodhead Publishing Series in Biomaterials, Applications of Nanocomposite Materials in Dentistry, Woodhead Publishing, 2019, Pages 1-25, ISBN 9780128137420

[5] McLaren EA, Figueira J. Updating Classifications of Ceramic Dental Materials: A Guide to Material Selection. Compend Contin Educ Dent. 2015 Jun;36(6):400-5; quiz 406, 416.

[6] Fu L, Engqvist H, Xia W. Glass-Ceramics in Dentistry: A Review. Materials (Basel). 2020 Feb 26;13(5):1049.

[7] Glass Ceramic Technology, Third Edition, Authors: Wolfram Holand, George H. Beall

[8] Graeser, S. (2005). Untersuchungen an Lithiumdisilikat

[9] Beuer, F.; Schweiger, J.; Edelhoff, D. Digital dentistry: An overview of recent developments for CAD/CAM generated restorations. Br. Dent. J. 2008, 204, 505–511.

[10] Poticny, D.J.; Klim, J. CAD/CAM In-office Technology. J. Am. Dent. Assoc. 2010, 141, 5S–9S.

[11] Bosch, G.; Ender, A.; Mehl, A. A 3-dimensional accuracy analysis of chairside CAD/CAM milling processes. J. Prosthet. Dent. 2014, 112, 1425–1431.

[12] Kirsch, C.; Ender, A.; Attin, T.; Mehl, A. Trueness of four different milling procedures used in dental CAD/CAM systems. Clin. Oral Investig. 2017, 21, 551–558.[13] Yin R, Jang YS, Lee MH, Bae TS. Comparative Evaluation of Mechanical Properties and Wear Ability of Five CAD/CAM Dental Blocks. Materials (Basel). 2019 Jul 12;12(14):2252.

[14] Willard A, Gabriel Chu TM. The science and application of IPS e.Max dental ceramic. Kaohsiung J Med Sci. 2018 Apr;34(4):238-242.

[15] Tysowsky GW. The science behind lithium disilicate: a metal-free alternative. Dent Today. 2009 Mar;28(3):112-3.

[16] Bindl A, Lüthy H, Mörmann WH. Thin-wall ceramic CAD/CAM crown copings: strength and fracture pattern. J Oral Rehabil. 2006 Jul;33(7):520-8.

[17] Brandt S, Winter A, Lauer HC, Kollmar F, Portscher-Kim SJ, Romanos GE. IPS e.max for All-Ceramic Restorations: Clinical Survival and Success Rates of Full-Coverage Crowns and Fixed Partial Dentures. Materials (Basel). 2019;12(3):462. Published 2019 Feb 2.

[18] Fasbinder DJ, Dennison JB, Heys D, Neiva G. A clinical evaluation of chairside lithium disilicate CAD/CAM crowns: a two-year report. J Am Dent Assoc. 2010 Jun;141 Suppl 2:10S-4S.

[19] French BM, Jezek PA, Appleman DE. Virgilite; a new lithium aluminum silicate mineral from the Macusani glass, Peru. American Mineralogist. 1978;63(5-6):461–465.

[20] Wang F, Yu T, Chen J. Biaxial flexural strength and translucent characteristics of dental lithium disilicate glass ceramics with different translucencies. J Prosthodont Res. 2020 Jan;64(1):71-77.

[21] Giordano RA 2nd, Pelletier L, Campbell S, Pober R. Flexural strength of an infused ceramic, glass ceramic, and feldspathic porcelain. J Prosthet Dent. 1995 May;73(5):411-8.

[22] Kansal R, Rani S, Kumar M, Kumar S, Issar G. Comparative Evaluation of Shear Bond Strength of Newer Resin Cement (RelyX Ultimate and RelyX U200) to Lithium Disilicate and Zirconia Ceramics as Influenced by Thermocycling. Contemp Clin Dent. 2018;9(4):601-606. doi:10.4103/ccd.ccd_601_18

[23] Baldissara P, Wandscher VF, Marchionatti AME, Parisi C, Monaco C, Ciocca L. Translucency of IPS e.max and cubic zirconia monolithic crowns. J Prosthet Dent. 2018 Aug;120(2):269-275

[24] Heffernan MJ, Aquilino SA, Diaz-Arnold AM, Haselton DR, Stanford CM, Vargas MA. Relative translucency of six all-ceramic systems. Part I: core materials. J Prosthet Dent. 2002 Jul;88(1):4-9.

[25] Heffernan MJ, Aquilino SA, Diaz-Arnold AM, Haselton DR, Stanford CM, Vargas MA. Relative translucency of six all-ceramic systems. Part II: core and veneer materials. J Prosthet Dent. 2002 Jul;88(1):10-5.

[26] Wang F, Takahashi H, Iwasaki N. Translucency of dental ceramics with different thicknesses. J Prosthet Dent. 2013 Jul;110(1):14-20.

[27] Wang CC, Fu PS, Wang JC, Lan TH, Lai PL, Du JK, Chen WC, Hung CC. Comparison of optical and crystal properties of three translucent yttria-stabilized tetragonal zirconia polycrystals with those of lithium disilicate glass-ceramic material. J Dent Sci. 2021 Oct;16(4):1247-1254.

[28] Luo XP, Zhang L. Effect of veneering techniques on color and translucency of Y-TZP. J Prosthodont. 2010 Aug;19(6):465-70.

[29] Scherrer SS, Quinn GD, Quinn JB. Fractographic failure analysis of a Procera AllCeram crown using stereo and scanning electron microscopy. Dent Mater. 2008 Aug;24(8):1107-13.

[30] Pick B, Meira JB, Driemeier L, Braga RR. A critical view on biaxial and short-beam uniaxial flexural strength tests applied to resin composites using Weibull, fractographic and finite element analyses. Dent Mater. 2010 Jan;26(1):83-90.

[31] Ban S, Anusavice KJ. Influence of test method on failure stress of brittle dental materials. J Dent Res 1990;69:1791–9.

[32] Jin J, Takahashi H, Iwasaki N. Effect of test method on flexural strength of recent dental ceramics. Dent Mater J2004;23:490–6

[33] Higgs WAJ, Lucksanasombool P, Higgs RJED, Swain MV.Evaluating acrylic and glass-ionomer cement strength using the biaxial flexure test. Biomaterials 2001;22:1583–90

[34] Chung SM, Yap AU, Chandra SP, Lim CT. Flexural strength of dental composite restoratives: comparison of biaxial and three-point bending test. J Biomed Mater Res B ApplBiomater 2004;71:278–83.

[35] Palin WM, Fleming GJ, Burke FJ, Marquis PM, Randall RC. The reliability in flexural strength testing of a novel dental composite. J Dent 2003;31:549–57.

[36] Eldwakhly E, Ahmed DRM, Soliman M, Abbas MM, Badrawy W. Color and translucency stability of novel restorative CAD/CAM materials. Dent Med Probl. 2019 Oct-Dec;56(4):349-356.

[37] Liebermann A, Mandl A, Eichberger M, Stawarczyk B. Impact of resin composite cement on color of computer-aided design/computer-aided manufacturing ceramics. J Esthet Restor Dent. 2021 Jul;33(5):786-794.

[38] Apel E, Van't Hoen C, Rheinberger V, Höland W. Influence of ZrO2 on the crystallization and properties of lithium disilicate glass-ceramics derived from a multi-component system J. Eur. Ceram. Soc., 27 (2007), pp. 1571-1577

[39] Stawarczyk B, Mandl A, Liebermann A. Modern CAD/CAM silicate ceramics, their translucency level and impact of hydrothermal aging on translucency, Martens hardness, biaxial flexural strength and their reliability. J Mech Behav Biomed Mater. 2021 Jun;118:104456

[40] Albero A, Pascual A, Camps I, Grau-Benitez M. Comparative characterization of a novel cad-cam polymer-infiltrated-ceramic-network. J Clin Exp Dent. 2015 Oct 1;7(4):e495-500.